DOI: 10.1007/s10535-017-0741-8 BIOLOGIA PLANTARUM 62 (1): 173-180, 2018

Changes in leaf tissue of *Carica papaya* during single and mixed infections with *Papaya ringspot virus* and *Papaya mosaic virus*

M.A. GARCÍA-VIERA, L. SÁNCHEZ-SEGURA, G. CHAVEZ-CALVILLO, D. JARQUÍN-ROSALES, and L. SILVA-ROSALES*

Departamento de Ingeniería Genética, Centro de Investigaciones y de Estudios Avanzados del IPN, Libramiento Norte Carretera Irapuato-León, 36821 Irapuato, México

Abstract

Papaya (*Carica papaya* L.) is susceptible to viral diseases caused by *Papaya mosaic virus* (PapMV) and *Papaya ringspot virus* (PRSV), which limit fruit production and affect economic yield. The symptoms produced by both the viruses are similar in early stages of infection and include vein and leaf chlorosis, which develop into mosaic at later stages of infection when leaf lamina can get reduced in size and distorted with a shoe-string aspect. Digital image analyses, such as fractal dimension (FD) and lacunarity (λ) were used here to examine papaya tissue after single and mixed infections of PRSV and PapMV. Morphological changes, such as hypoplasia, hyperplasia, and neoplasia are described in tissues with viral infections. Furthermore, we quantified these changes and suggest three ranges of tissue damage according to their λ values in rank 1 (0.01 to 0.39), rank 2 (0.4 to 0.79), and rank 3 (0.8 to 1). Our analyses suggest that in synergism and antagonism there is a competition of both viruses to occupy the same mesophyll cells, as indicated by their intermediate values of lacunarity.

Additional key words: antagonism, digital image analyses, fractal dimension, histology, lacunarity, synergism.

Introduction

Papaya (*Carica papaya* L.) is an important crop in India, Brazil, Indonesia, Dominican Republic, Nigeria, and Mexico. Papaya fruit yield is affected by diseases caused by many viruses (Lebsky *et al*. 2010), including *Papaya ringspot virus* (PRSV) and *Papaya mosaic virus* (PapMV) (Noa-Carrazana *et al*. 2006). In Mexico, PRSV was first reported by Teliz *et al*. (1991) and PapMV was discovered by Noa-Carrazana and Silva-Rosales (2001). PRSV is a member of the genus *Potyvirus* in the *Potyviridae* family, with 700 - 900 nm long filamentous particles (Tripathi *et al*. 2008). PapMV belongs to the *Alphaflexiviridae* family and has 530 nm long filamentous particles (Noa-Carrazana *et al*. 2006). The chlorotic spots and vein clearing symptoms produced by PapMV and PRSV at early stages of infection are very similar (Noa-Carrazana *et al*. 2006). However, oily streaks are only produced on the stem by PRSV infections. At later stages of infection, leaf distortion and concentric rings on mature and ripened fruits can be observed (Cruz *et al*. 2009). Both PRSV and PapMV can infect plants in mixed infections, producing synergism or antagonism as reported recently by Chávez-Calvillo *et al.* (2016) depending upon the first virus infection.

The infections by both PRSV and PapMV have been diagnosed by conventional techniques like ELISA and reverse-transcription (RT)-PCR (Noa-Carrazana *et al*. 2006, Tuo *et al*. 2014). To carry out this diagnostic procedure, the tissue needs to be disrupted and subcellular content homogenized in the sample. Another approaches to dissect, detect, and study viral infections in plant tissues are histological techniques (Evert 2006). However, few researchers identify, quantify, and evaluate tissue morphology based on acquired images as alternative diagnosis of viral pathologies, despite being a process facilitating cytopathic discrimination and qualitatively describing the symptoms. The quantification of histological features is not a straightforward procedure and only few such techniques are suitable to evaluate the changes in anatomy of affected tissue (Guines *et al*. 2003, Guillemin *et al*. 2011). Recent reports show that plant

Submitted 24 January 2016, *last revision* 27 March 2017, *accepted* 28 March 2017.
Abbreviations: A - area, DIA - digital image analyses, Fe - feret diameter, FD - fractal dimension, λ - lacunarity, PRSV - *Papaya ringspot virus*, PapMV - *Papaya mosaic virus*, VB - vascular bundle.
Acknowledgements: We acknowledge the *Cinvestav* greenhouse staff and the SAGARPA-CONACYT- 2011-02-163213 project funding.
* Corresponding author; fax: (+52) 462 6239651, e-mail: lsilva@ira.cinvestav.mx

histology can be studied through fractal dimension (FD) (Chanona *et al.* 2003, Gumeta-Chávez *et al.* 2011, Utrilla-Coello *et al.* 2013). This method allows the measurement of irregular shapes of objects and is based on self-similarity of fractal geometry (Mandelbrot 1983, Ross 2005, Milosevic and Ristanović 2009). One method to calculate FD is box counting, with progressively larger boxes of side length, superimposed to the image of interest and then finding FD as the absolute value of the slope of the logarithmic plot of the number of boxes (N) *vs*. the box size (ε) (Borys *et al.* 2008). The FD is calculated using the following equation (1).

$$FD = \frac{1}{1-q}\ lim_{\varepsilon \to 0}\ \frac{log\ \sum_{t=1}^{n} \mu_i^q}{log\frac{1}{\varepsilon}} \qquad (1)$$

where q is dimension index (q = 0) and μ is pixel density. However, some images display different areas that do not correspond to pixel constitution of the object and therefore this information is not considered in the FD measure. To counterbalance this pixel underestimation, Mandelbrot (1983) developed the lacunarity (λ) theory that describes the distribution of spaces or gaps in a certain image that are not filled (totally or partially) by the superimposed boxes of the FD (Kilic and Abiyev 2011). Lacunarity is a relatively new feature to aid in the description of morphological changes of objects (Borys *et al.* 2008) and is calculated by the following equation (2) (Borys *et al.* 2008),

$$\lambda = \frac{E(X^2)}{(EX)^2} = \frac{D^2X+(EX)^2}{(EX)^2} = 1 + \frac{D^2X}{(EX)^2} = 1 + \lambda \qquad (2)$$

where $E\ [X]$ is the expected value of X (X - number of holes or black pixels) and D^2X is the variance of X (Borys *et al.* 2008).

In this study, we describe the morphological effects of single and mixed infections (resulting in synergism and antagonism) of PRSV and PapMV on plant tissue. For each infection type, an association of their fractal dimension and lacunarity was analysed on the microscopic images of leaf tissue sections. These two parameters allowed the classification and assessment of the infection of these two viruses in the leaf tissue.

Materials and methods

Plant growth and inoculation: The seeds of *Carica papaya* L. cv. Maradol were sown in germination substrate containing 1:1 (v/v) coconut paste and *Sunshine Mix 1-LC1* (*Sungro Horticulture*®, Massachusetts, USA). When cotyledonary leaves emerged, the seedlings were transplanted into soil with adequate irrigation and fertilization. All plants were grown in a greenhouse under day/night temperatures of 28/17 ºC, a relative humidity of 45 - 85 %, a 12-h photoperiod, and an irradiance of 700 - 1 100 μmol m^{-2} s^{-1}. Six-week-old plants were selected for all experiments. The identity of the inoculated viruses PRSV, isolate VrPO (AY231130) and PapMV, isolate GTO, was confirmed by enzyme linked immunosorbent assay (ELISA) using antibodies produced against coat protein (CP) (Agdia - α-PapMV 53400/1000 and α-PRSV 53500/1000) and reverse transcription (RT)-PCR by amplifying the *CP* gene of both the viruses (Chávez-Calvillo *et al*. 2016).

The virus infected plant tissue was ground in cold (4 °C) 0.001 M sodium phosphate buffer (pH 8.0) containing 0.001 M EDTA. The extract was filtered through a double layer of muslin cloth. The infection of viruses was carried out in the third leaf of each plant aided with dusted carborundum (400 mesh, *Troemner*, New Jersey, USA). A piece of sterile cotton dipped in filtrate was rubbed unidirectionally on the upper surface of the leaves supported with a piece of cardboard under the lower surface to avoid leaf injury. The inoculated leaves were washed immediately with a jet of sterile water to remove traces of carborundum. The plants were labelled and kept for observations. The ELISA test was conducted on mechanically inoculated plants to detect the presence of a virus. The concentration of the inoculated virus in the tissue was calculated based on a calibration curve plotted using values of five concentrations of pure virus as a standard, and the fluorescence crossing points in RT-quantitative (q)PCR, through a linear regression model, as explained in a later section.

The order of mock, single, or mixed inoculations, for the synergistic or antagonistic interactions, was as follows: mock infection was only inoculated with sodium phosphate-EDTA buffer, PapMV infection was inoculated using viral particles of PapMV-GTO, and PRSV infection was inoculated with viral particles of PRSV-P-VrPO (AY231130); in synergism interactions (PRSV→PapMV), PRSV infected plants were infected with viral particles of PapMV at 30 d post infection of the first virus. In antagonism interactions (PapMV→PRSV), PapMV infected plants were infected with viral particles of PRSV at 30 d post infection of the first virus.

RT-qPCR: RNA was extracted from healthy and infected plants at 60 d post-inoculation (dpi) using *Trizol* reagent (*Invitrogen*, Carlsbad, USA). The extraction was followed by a *DNaseI* (*Invitrogen*) treatment to eliminate any possible DNA contamination. The quality and quantity of the RNA were evaluated with a *NanoDrop* spectrophotometer (*Thermo Fisher Scientific*, San Jose, CA, USA) using the absorbance ratios 260/280 nm and 260/230 nm.

RNA integrity was also checked by electrophoresis on a 1 % (m/v) agarose gel stained with *GelRed* (*Biotium*, Fremont, USA). A total of 500 ng of RNA was used for the synthesis of the first strand cDNA using 200 U of *SuperScript*^{III} (*Invitrogen*) per reaction. The cDNA generated was used for the next PCR reaction, the primer pairs 458-btub-F/459-βtub-R, 773-PapMV-01-F/774-PapMV-01-R, and 775-PRSV-F/776-PRSV-R (see Table

1 Suppl.) were used in a multiplex RT-PCR standard reaction for for 1 cycle of 94 °C for 1 s, and 35 cycles (each of 15 s at 94 °C, 30 s at 60 °C, 35 s at 73 °C), and final extension at 72 °C for 1 min. The amplification of the *β-tubulin*, RNA dependent RNA polymerase (RdRp), and the CP fragments of PapMV and PRSV, respectively, were run on a 1 % agarose gel stained with *GelRed*.

Histology of leaves: For histological studies, ten leaf samples were collected from three plants of each treatment at 60 dpi. The samples were cut with a hole-puncher (diameter 5 mm) and fixed in a FAA solution consisting of formaldehyde + acetic acid glacial + 100 % ethanol + deionized water in the ratio 50:5:10:35 (v/v/v/v/) for about 12 h. The fixed material was dehydrated through a graded ethanol (40 to 100 %) for 30 min for each step at room temperature. The infiltration was carried out in ethanol-xylene solution, in ratios of 2:1, 1:1 and 1:2 (v/v), for 1 h in each solution and embedded in paraffin wax (*Paraplast*®, Richmond, USA) at 60 °C. The embedded tissues were cut, using a rotary microtome (*LKB*, Bromma, Sweden), at 10 µm thickness. The paraffin ribbons were dewaxed in a xylol-ethanol series and the sections were then stained with Ruthenium Red (0.5 mg cm^{-3}) (*Sigma-Aldrich*, St. Louis, USA) for pectin detection, and with Coomassie Brilliant Blue R-250 (0.01 g cm^{-3}) (*Sigma-Aldrich*), dissolved in a 50 % ethanol solution for protein staining, followed by permanent mounting using *Entellan*® resin (*Merck*, Darmstadt, Germany) and for their further observation under the optical microscope (*Leica DM6000-B*, Benstein, Germany).

Digital image analysis (DIA): After histological processing, the DIA was carried out according to Sánchez-Segura *et al*. (2015). The sizes of the images were 2560 × 1920 pixels and were captured as RGB colour format. The image resolution was 0.29 pixels μm^{-2}. The mesophyll tissue image was segmented as needed using the immunohistochemistry (IHC) image plugin (National Institutes of Health, Bethesda, MD, USA). All images were captured at 10× according to Sánchez-Segura *et al.* (2015) with the *Analysis Toolbox of ImageJ 1.48* software. This method allowed the detection of morphological modifications in the mesophyll tissue and enabled the analysis of features of the histological slices. Area (A) and Feret diameter (Fe) were calculated using the *ImageJ* software. The fractal dimension (FD) and lacunarity (λ) were calculated by using the box-counting method (*FracLac_2.5 released version 1.0 for Image J*); FD is an index of mass compactness, while λ is a quantifier of the heterogeneity or compactness of structure (Utrilla-Coello *et al*. 2013). In this work, λ was used to qualitatively describe the responses produced by PapMV and PRSV in single and mixed infections as compared to the healthy tissues. The Feret diameter (Fe) is a function of the area and is called fractal area (A_F) related through the FD on the powered expression, as reported before (Olsen *et al.* 1993): $A_F \alpha (Fe)^{FD}$.

Results

Carica. papaya plants with the mock inoculation showed a normal development (Fig. 1*A*). Plants inoculated with PapMV had contrasting mosaics and some small bulgings in proximity to the veins (Fig. 1*B*). Plants infected with PRSV showed mosaics, chlorosis, rugosities, stripes, shrinkage, and distortion of young leaves. These symptoms indicate abnormal leaf development (Fig. 1*D*). However, we found that the stepwise inoculations of PapMV followed by PRSV affected the phenotype of the infected plants. The symptoms attributed to antagonism infection were chlorosis, vein clearing, and mosaics (Fig. 1*C*). These symptoms are like PapMV infections at the early stages of the disease and never have a striking effect on the plant as those produced by PRSV (Chávez-Calvillo *et al*. 2016). Plants infected with PRSV followed by PapMV resulted in viral synergism. The phenotype observed as an abnormal development in leaves similar to advanced stages of those produced by PRSV disease but more damaging to the plant than the single infection (Fig. 1*E*).

The presence of the PapMV and PRSV viral genomes was evidenced by the amplification of a fragment of the *PapMV RdRP* and/or the *PRSV CP*, and the additional *β-tubulin* gene was included as a positive control of the multiplex RT-PCR reaction. The multiplex RT-PCR reaction successfully detected *PapMV* and *PRSV* in the tissue samples and they did not cross-react (Fig. 2). The plants singly inoculated showed the presence of *PapMV* or *PRSV* only (Fig. 2). However, the two-step infections (PapMV→PRSV and PRSV→PapMV) undergoing antagonism and synergism, respectively, showed the presence of both viruses in systemic tissue (Fig. 2). The results of this molecular diagnosis confirmed the PapMV and PRSV infection on the systemic tissue in plants undergoing the antagonistic or synergistic interaction.

The transverse sections of healthy plants of *C. papaya* showed a normal leaf anatomy: an upper epidermis, a mesophyll tissue, and a lower epidermis (Fig. 3*A*). Vascular bundles (VB) showed ring arrangements with two VB positioned one on the upper side and the other on the lower side (Fig. 3*A*). The laminar mesophyll region was differentiated into upper palisade and lower spongy tissues. Palisade mesophyll was formed by two rows with cells of approximately 10 × 2 µm. The spongy tissue consisted of 5 - 6 layers of cells as stated before (Zunjar *et al*. 2011). Plants inoculated with PapMV showed symptoms at 10 dpi. The affected areas extended to the superior leaves when the infection was systemically established. In the first histological proximal slices of each paraffin block, the normal constitution of the cells of

the mesophyll tissue was observed (Fig. 3*A*). However, in histological Z-stack reconstruction (tissue slices were cut in depth), the progress of leaf deformation was observed in the samples. This deformation was due to an increase in the size of the VB and hyperplasia of the sieve elements (Fig. 3*B*-*C*). Protein staining was observed in cells of the mesophyll tissue and the VB (Fig. 3*C*-*D*).

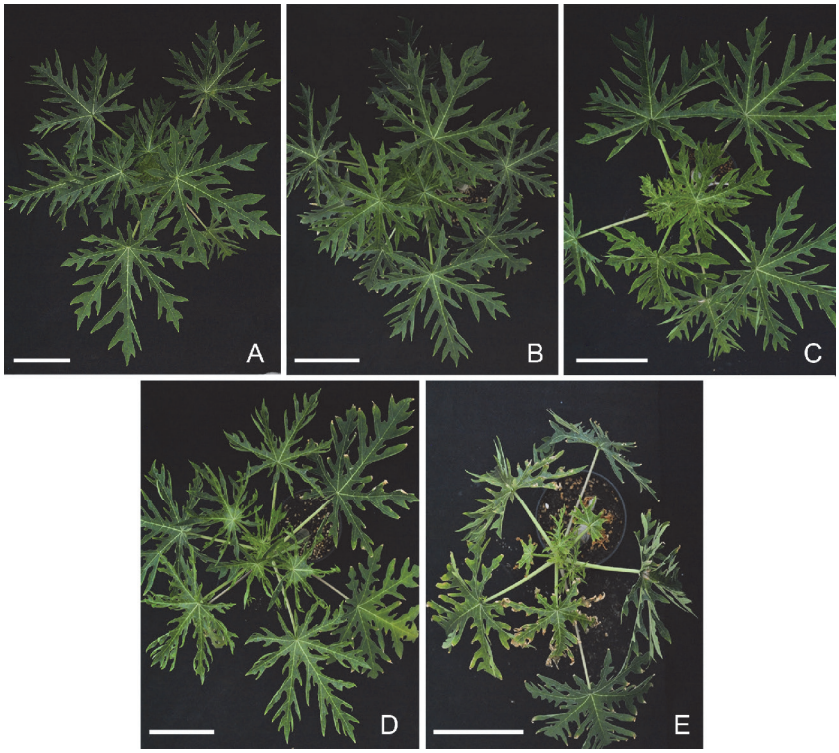

Fig. 1. Symptom development in papaya infected plants. Representative phenotypes of mock-inoculated (*A*), PapMV (*B*) or PRSV (*D*) inoculated plants at day 0 and PapMV inoculated plants at day 0 and PRSV re-inoculated at day 30 (PapMV→PRSV), which resulted in viral antagonism with decreased symptoms and no leaf deformation or foliar mass losses (*C*). PRSV inoculated plants in day 0 and *PapMV* re-inoculated 30 days later (PRSV→PapMV), which resulted in viral synergism with severe necrosis and foliar mass loss (*E*). Photographs were taken at 60 dpi, *bar* = 20 cm.

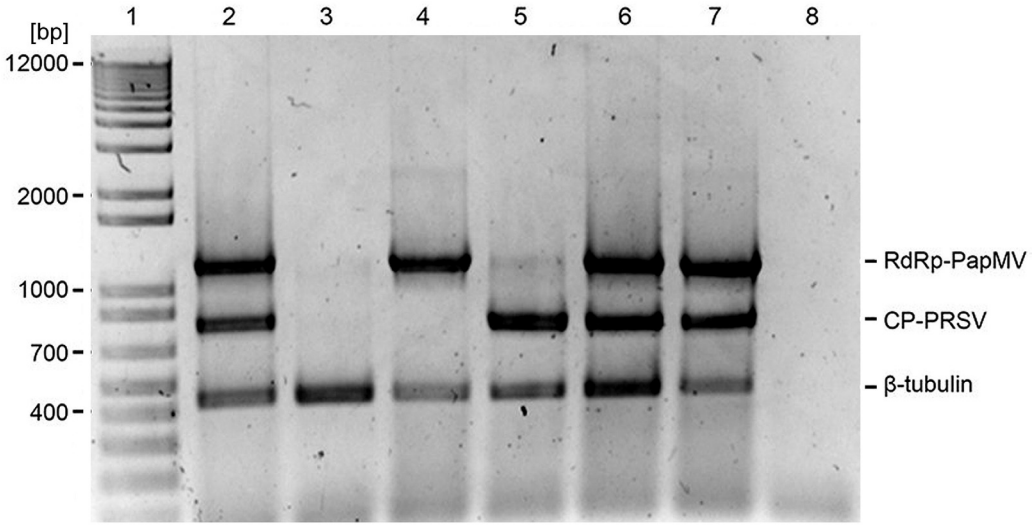

Fig. 2. Presence of PRSV and PapMV. Accumulation of the *RdRp-PapMV* (1 200 bp), *CP-PRSV* (800 bp), and the *β-tubulin* gene (450 bp) as the loading control detected by RT-PCR. *Lane* 1 - DNA ladder (*Invitrogen*); *lane* 2 - positive control for the home in-built multiplex detection kit; *lane* 3 - healthy plant; *lane* 4 - PapMV infected plant; *lane* 5 - PRSV infected plant, *lane* 6 - PRSV infected plants re-inoculated with PapMV 30 d later (PRSV→PapMV); *line* 7 - PapMV infected plants re-inoculated with PRSV 30 d later (PapMV→PRSV); and *lane* 8 indicates the negative control.

In histological observations, the plants infected with PRSV showed a main effect in the parenchymal tissue. This tissue showed increase of cell size as compared to PapMV-infected leaves, and it was also more compact without intercellular spaces (Fig. 3*E*). The malformation of the leaf seems to be due to an increase in the size of the vascular tissue or to an hyperplasia of the parenchyma cells. Cell areas without a profuse protein staining were also observed (Fig. 3*E*). Therefore, the stained area of the mesophyll tissue decreased in proportion to that of the palisade parenchyma (Fig. 3*F*) accompanied with the strong leaf chlorosis, distinctive of this type of infection. Low content of proteins was observed in mesophyll and in the VB (Fig. 3*F*).

The histological images of leaves with antagonistic phenotype showed protein accumulation in the mesophyll cells (Fig. 4*A,B*) and the VB (Fig. 4*B*). The parenchymal tissue appeared disorganised (Fig. 4*A-B*) as compared to mesophyll tissue from a healthy plant (3*A*). In histological observations in the synergistic condition, we observed the reduction of the leaf area (Fig. 4*C-D*), with the parenchymal cells decreased in size and abnormal morphology, as compared to tissue of infected leaves with PRSV or PapMV. The mesophyll tissue showed lower blue staining but the protein accumulation was observed in VB (Fig. 3*F*). In spongy and mesophyll tissues, a higher compactness (Fig. 4*C-D*) was observed with irregular distribution of cells as well as intercellular spaces.

The images captured from the histological analyses were segmented with the IHC tool by isolating specific areas stained in red-pink colour (data not shown). These

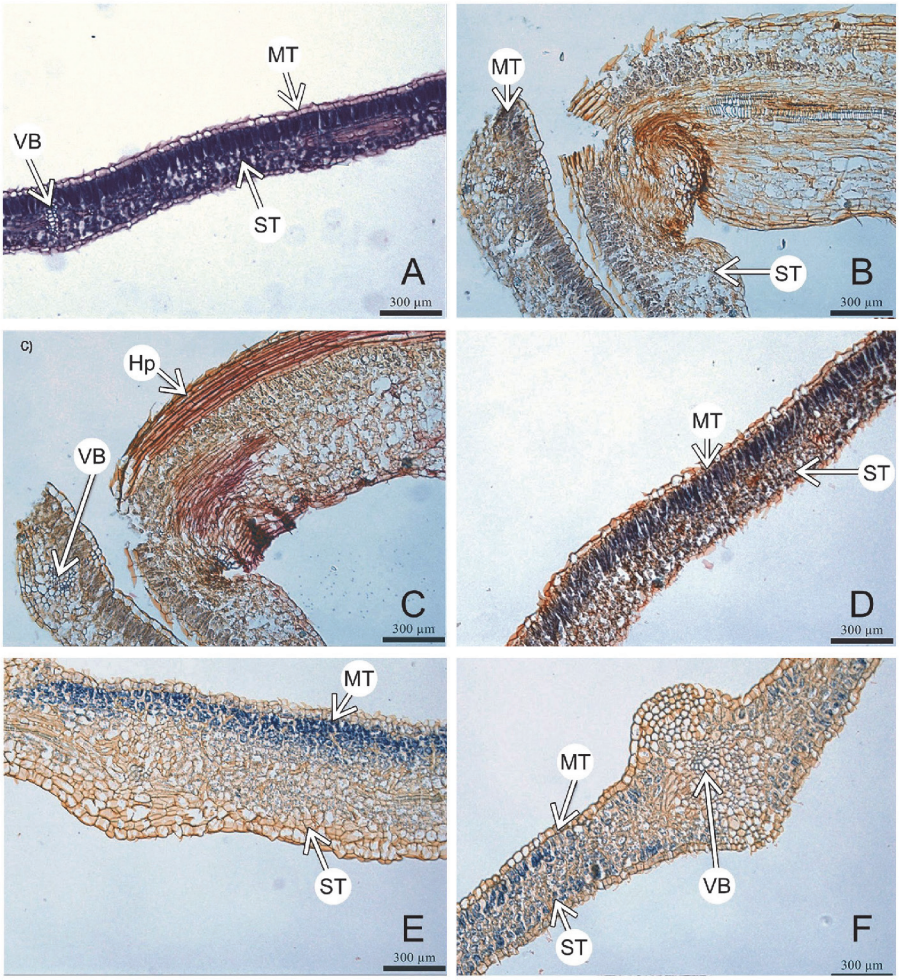

Fig. 3. Leaf cross sections from a healthy plant *(A)* and PapMV (*B-D*) and PRSV (*E-F*) infected plants. *A* - Transversal leaf section with normal disposition of mesophyll tissue (MT) stained for proteins (*blue*). Spongy tissue (ST) showing intercellular spaces and vascular bundles (VB). *B* - The first slices with a normal disposition of mesophyll tissue (MT) in the PapMV infected leaf. *C* - Distal slices towards a damaged area, a hyperplasia (Hp) of the sieve elements is present. *D* - Protein staining in palisade parenchyma (*blue stained*) was observed in *B-D* images. A minor protein stained area in the vascular bundle (VB, Fig. *C*). *E* - Spongy cells increased in size (ST, in *orange*) with respect to cells from mesophyll tissue (MT, in *blue*). *F* - Distorted young leaves with chlorotic spots showing irregular disposition of parenchymal tissue and decreased number of mesophyll cells. The accumulation of protein (*blue* stained) in palisade and spongy parenchyma cells are reduced as compared to healthy leaves.

areas were associated with infection (cells with neoplastic features). The subsequent images without red-pink staining and positive for the blue staining (protein) showed alterations in size and shape (data not shown). In the binary images (black and white), the black pixels represented mesophyll tissue areas affected by the infection whereas white pixels corresponded to the absence of parenchyma tissue (Z-stack, data not shown).

In these segments of images, FD and λ were measured. In this study, the FD was used to estimate changes associated with viral infection and compared to healthy tissues. Lacunarity values showed changes for the viral infections. Each infection presented characteristic average values of FD and λ: for mock treatment (FD = 1.702 ± 0.118 and λ = 0.253 ± 0.064), for PapMV infection (FD = 1.494 ± 0.086 and λ = 0.799 ± 0.282), for PRSV infection (FD = 1.487 ± 0.232 and λ = 0.806 ± 0.319), for the antagonistic mixed infection (FD = 1.460 ± 0.130 and λ = 0.648 ± 0.301) and finally, for the synergistic infection (FD = 1.572 ± 0.095 and λ = 0.445 ± 0.157). Thus, FD and λ had their highest and lowest values in healthy tissues (Fig. 1 Suppl.), they remained inversely proportional in the treatments of single (PapMV and PRSV) and double infection showing antagonism but not those showing synergism. We estimated correlation coefficients (cc) between the A_F (Eq. (3) and average tissue areas, A_T, for the infected and non-infected tissue segments. The cc values were 0.893, 0.542, and 0.629 for PRSV infection, antagonism, and synergism, respectively; whereas for mock and PapMV, no significant correlation was found. The cc values increased in the presence of PRSV virus or in the combination of PRSV with other virus in the mesophyll tissue. The result of the interactions between PRSV and other virus was seen in the spongy mesophyll tissue as a decrease in its area, as compared to the parenchymal tissue. The lacunarity behaviour of virus interactions showed different trends in relation to the mock or single PapMV and PRSV infections. This behaviour indicated that the leaf tissue structure with mock infection is rather homogeneous and was placed in range 1 with λ between 0.01 to 0.39 (Fig. 1 Suppl.). Lacunarity behaviour in the interaction of the plant with the single PapMV or PRSV infections showed a tissue heterogeneity limit with range 3 having λ between 0.8 and 1 (Fig. 1 Suppl.). However, in both antagonism (PapMV→PRSV) and synergism (PRSV→PapMV), the tissue heterogeneity had the intermediate range of 2 with a λ between 0.4 to 0.79 (Fig. 1 Suppl.).

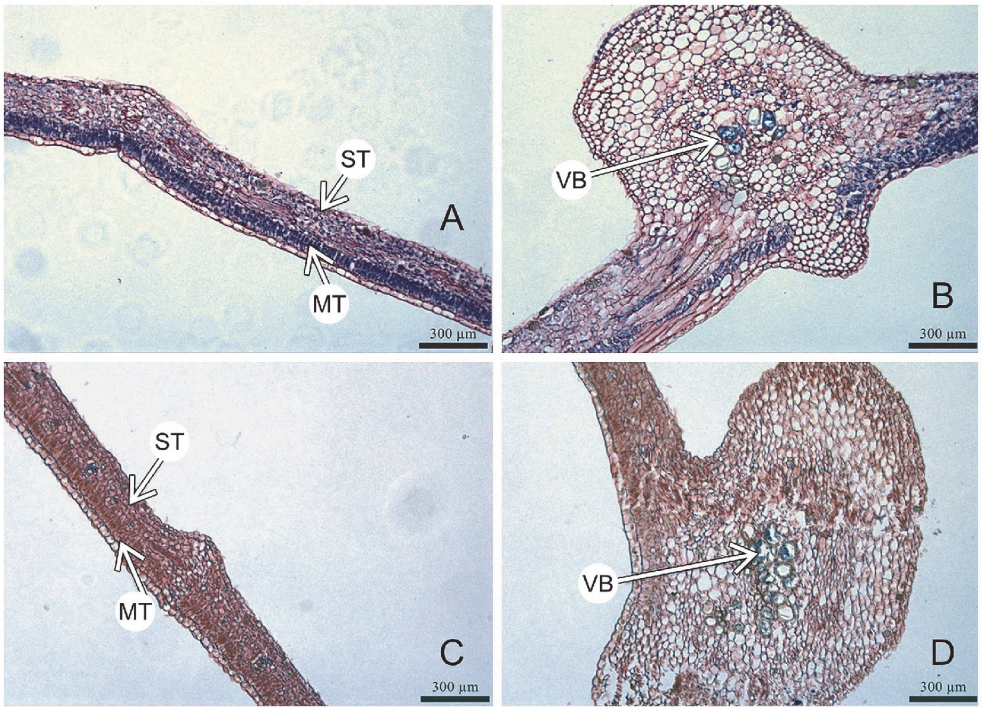

Fig. 4. Leaf cross sections from plant with the sequential infection of PapMV→PRSV (showing antagonism, *A-B)* and PRSV→PapMV (showing synergism, *C-D)*. Accumulation of protein (*blue stained*) in palisade and spongy parenchyma cells (*A-B*), are reduced as compared to healthy leaves (showed in Fig. 3*A*), Spongy tissue (ST) increased in area as compared to the mesophyll tissue (MT) and protein accumulation in the vascular bundle and the mesophyll tissues (VB and MT). *C* - Spongy tissue (ST) increased in size (at the far right) as compared to the mesophyll tissue (MT, in the left side of the tissue with *blue* areas). *D* - Irregular disposition of parenchymal tissue and decreased size of mesophyll cells and increased protein accumulation in the vascular bundle (VB).

Discussion

During virus infection, different phenotypes are observed depending on the interaction with the host and the virus strain. In a previous study, we showed that mixed infections by PRSV and PapMV are common in papaya and could lead to antagonism or synergism depending on the order of inoculation (Fig. 1 and Chávez-Calvillo *et al*. 2016). These phenotypes are still poorly understood. The scrutiny of the infection in plant tissues by histological techniques provides information on the tissue disruption associated to the single (PRSV or PapMV), or stepwise (PapMV→PRSV and PRSV→PapMV) inoculations leading to antagonism or synergism, respectively (Shand *et al*. 2009). The infection with PapMV resulted in total protein content in mesophyll and spongy parenchyma cells like under mock inoculation (Fig. 3*D*). However, at this infection, we observed an increase in the size of the vascular bundles and hyperplasia of the sieve elements suggesting a virus presence and therefore its possible movement in this tissue (Fig. 3*B*-*C*). In the PRSV infection, the accumulation of protein in mesophyll and spongy parenchyma cells was reduced as compared to the healthy leaf. These results are consistent with those previously reported (Kunkalikar *et al*. 2007). The histological studies showed a reduced mesophyll area due to disorganisation and increase in the size (hypertrophy) of the spongy parenchyma cells (Fig. 3*E*-*F*) similar to those reported in diseased tobacco and papaya leaves (Shand *et al*. 2009, Singh and Shukla 2012). Kunkalikar *et al*. (2007) suggested that the reduction in size (hypotrophy), in mesophyll and spongy parenchyma cells, as well as their destruction, could be due to metabolic changes in these cells. PRSV might produce chlorosis as the result of the lower density and size of mesophyll parenchyma cells. Similar results have been reported by Singh and Shukla (2012), who suggested that the smaller mesophyll cells and degeneration of chloroplasts induced gradual chlorosis. The synergistic infections by *Potyvirus* and *Potexvirus* were reported by Pruss (1997) and Pacheco (2012) but without histological observations. After PRSV→PapMV infection we observed a low staining of protein and the distribution of tissues like healthy plants (Fig. 4*C*-*D*). However, the mesophyll and parenchymal tissues showed hypotrophy and neoplasia in a similar way to the PRSV infection (Fig. 4*C*-*D*). Also, the parenchymal cells in the tissues formed interstitial spaces that have been reported in tobacco tissue infected with *Potato virus Y* (PVY) (Shand *et al*. 2009). Under the antagonistic conditions, the histological images showed protein accumulation in the mesophyll cells and the vascular bundles (Fig. 4*A*-*B*). Hypertrophy was observed in the parenchymal tissues and hypotrophy in the mesophyll cells (Fig. 3*G*). The accumulation of total protein in the vascular bundle was neither seen in the synergism nor in the single PapMV and PRSV infections (Fig. 4*B*). The VB is an important component of the transport system in vascular plants. After mechanical inoculations, the virus moves from the epidermis to the mesophyll cells. Further cell-to-cell (plasmodesmata) and long-distance (phloem) movement (Hipper *et al*. 2013) take place. In *Potexvirus*, the CP and triple gen block 1 (TGB1) are required for cell-to-cell and long-distance movement (Cruz *et al*. 1998, Lough *et al*. 2001). The *Potyvirus* infection requires CPs (VPg-pro, HC-Pro, and 6K2) for long-distance movement (Hipper *et al*. 2013). It is tantalizing to speculate that the presence of total protein in the vascular bundle is due in part by the by the translocation of viral proteins considering an increase of viral CP in the antagonistic response (Chávez-Calvillo *et al*. 2016). Immunolocalization assays will help us to discern the type of protein abundance in this tissue. To get a deeper understanding of the morphological changes of the affected leaf tissues in the different types of viral infections, we measured fractal dimension and lacunarity. These parameters have not been regularly used in phytopathology and more specifically in plant-virus interactions that we are aware of. Fractal theory has been applied to a variety of landscape ecology problems because they conveniently describe many of the irregular, fragmented patterns found in nature (Mandelbrot 1983). More recently, the lacunarity analysis on images was used for texture classification of different patterns in agricultural studies (Li *et al*. 2014, Quan *et al*. 2014). We identified changes as hypoplasia, hyperplasia, and neoplasia in leaf tissues allowing us to discriminate cytopathic effects on the tissues due to single and mixed viral infections and qualitatively describe the symptoms of those infections. The big differences between antagonism and synergism, in terms of their relationship of FD and λ (Fig. 1 Suppl.), reflect a higher heterogeneity and irregularity of tissues. Mesophyll tissue identity was preserved more in the antagonistic interaction (Fig. 4*A*,C), similar to the mock plants, than in the synergistic interactions. This would suggest that there was a competition of both viruses to occupy the mesophyll tissue. Both PRSV and PapMV viruses colonise the mesophyll tissue so that the analysis of λ shows patterns describing an intermediate heterogeneity. According to the evaluation of λ (Fig. 1*B* Suppl.), ranges correspond to single and mixed viral infections. The intermediate λ (range 2) in mixed infections (Fig. 1*B* Suppl.) could be the result of a structural tissue resilience to preserve its homogeneity. As far as we are aware of, this is the first case when a direct implication of λ is attached to a biological system. The histological techniques used for evaluation of cell morphological features provided useful information on the organisation at ultrastructural and cellular levels (Evert 2006) in single and mixed infections. Unfortu-nately, there are few reports that identify and evaluate tissue morphology based on acquisition images. In addition, using these types of approaches as alternative strategies for diagnosis, provides a useful insight into cytopathic effects caused by different types of viral infections. It appears that this is a first report where DIA has been used for identification of

virus infection in plants as at the cellular level caused by mixed viral infections. Consequently, we proved the effecti-veness of this methodology to evaluate the morphology of infected tissues in single and mixed viral infections.

References

Borys, P., Krasowska, M., Grzywna, J.Z., Djamgoz, B.A., Mycielska, E.M.: Lacunarity as a novel measure of cancer cells behaviour. - BioSystems **94**: 276-281, 2008.

Chanona, P.J.J., Alamilla, B.L., Farrera, R.R.R., Quevedo, R., Aguilera, J.M., Gutiérrez, L.F.G.: Description of the convective air-drying of a food model by means of the fractal theory. - Food Sci. Technol. Int. **9**: 0207-0213, 2003.

Chávez-Calvillo G., Contreras-Paredes A.C., Mora-Macias J., Noa-Carrazana C.J., Serrano-Rubio A.A., Dinkova D.T., Carrillo-Tripp M., Silva-Rosales L.: Antagonism or synergism between papaya ringspot virus and papaya mosaic virus in *Carica papaya* is determined by their order of infection. - Virology **489**: 179-191, 2016.

Cruz, F.C., Tañada, J.M., Elvira, V.P.R., Dolores, L.M., Magdalita, P.M., Hautea, D.M., Hautea, R.A.: Detection of mixed virus infection with *Papaya ringspot virus* (PRSV) in papaya (*Carica Papaya* L.) grown in Luzon, Philippines. - Philipp. J Crop Sci. **34**: 62-74, 2009.

Cruz, S.S., Roberts, A.G., Prior, D.A.M., Chapman S., Oparka, K.J.: Cell-to-cell and phloem-mediated transport of *Potato virus X*: the role of virions. - Plant Cell **10**: 495-510, 1998.

Evert, R.F. (ed.): Esau's Plant anatomy. Meristems, Cells, and Tissues of the Plant Body: their Structure, Function, and Development. - John Wiley & Sons, Hoboken 2006.

Guillemin, F., Devaux, M.F., Guillon, F.: Evaluation of plant histology by automatic clustering based on individual cell morphological features. - Image Anal. Stereol. **23**: 13-22, 2011.

Guines, F., Julier, B., Ecalle, C., Huyghe, C.: Among and within-cultivar variability for histological traits of lucerne (*Medicago Sativa* L.) stem. - Euphytica **130**: 293-301, 2003.

Gumeta-Chávez, C., Chanona-Pérez, J.J. Mendoza-Pérez, J.A. Terrés-Rojas, E., Garibay-Febles, V., Gutiérrez-López, F.G.: Shrinkage and deformation of *Agave atrovirens* Karw tissue during convective drying: influence of structural arrange-ments. - Dry Technol. **29**: 612-623, 2011.

Hipper, C., Véronique, B., Ziegler-Graff, V., Revers, F.: Viral and cellular factors involved in phloem transport of plant viruses. - Front. Plant Sci. **4**: 154, 2013.

Kilic, I.K., Abiyev, H.R.: Exploiting the synergy between fractal dimension and lacunarity for improved texture recognition. - Signal. Process. **91**: 2332-2344, 2011.

Kunkalikar, S., Byadgi, A.S., Kulkarni, V.R., Krishnareddy, M. Prabhakar, A.S.N.: Histopathology and histochemistry of papaya ringspot disease in papaya. - Indian J. Virol. **18**: 33-35, 2007.

Lebsky, V., Poghosyan, A., Silva-Rosales, L.: Application of scanning electron microscopy for diagnosing phytoplasmas in single and mixed (virus-phytoplasma) infection in papaya. - Julius-Kühn Archiv. **427**: 70-78, 2010.

Li, L., Zhang, Q., Huang, H.: A review of imaging techniques for plant phenotyping. - Sensor **14**: 20078-20111, 2014.

Lough, T.J., Emerson, S.J., Lucas, W.J., Forster, R.L.: Trans-complementation of long-distance movement of *White clover mosaic virus* triple gene block (TGB) mutants: phloem-associated movement of TGBp1. - Virology **288**: 18-28, 2001.

Mandelbrot, B.B. (ed.): The Fractal Geometry of Nature. - Freeman, W.H. and Company, New York 1983.

Milosevic, N.T., Ristanović, D.: Cell image area as a tool for neuronal classification. - J. Neurosci. Methods **182**: 272-278, 2009.

Noa-Carrazana, J.C., González-de-León, D., Ruiz-Castro, B.S., Piñero, D., Silva-Rosales, L.: Distribution of *Papaya ringspot virus* and *Papaya mosaic virus* in papaya plants (*Carica papaya*) in Mexico. - Plant Dis. **90**: 1004-1011, 2006.

Noa-Carrazana, J.C., Silva-Rosales, L.: First report of a Mexican isolate of *Papaya mosaic virus* in papaya (*Carica Papaya*) and pumpkin (*Cucurbita Pepo*). - Plant Dis. **85**: 558, 2001.

Pacheco, R., García-Marcos, A., Barajas, D., Martiáñez, J., Tenllado, F.: *PVX-Potyvirus* synergistic infections differentially alter microRNA accumulation in *Nicotiana benthamiana*. - Virus Res. **165**: 231-235, 2012.

Pruss, G., Ge, X., Shi, X.M., Carrington, J.C., Bowman Vance, V.: Plant viral synergism: the potyviral genome encodes a broad-range pathogenicity enhancer that transactivates replication of heterologous viruses. - Plant Cell **9**: 859-868, 1997.

Quan, Y., Xu, Y., Sun, Y., L, Y.: Lacunarity analysis on image patterns for texture classification. - In: editor? (ed.): 2014 IEEE Conference on Computer Vision and Pattern Recognition (CVPR). Pp. 160-167. CVPR-IEEE 2014.

Ross, M.C.: A new way of describing meiosis that uses fractal dimension to predict metaphase I. - Int. J. Biol. Sci. **1**: 123-125, 2005.

Sánchez-Segura, L., Téllez-Medina, D.I., Evangelista-Lozano, S., García-Armenta, E., Alamilla-Beltrán, L., Jiménez-Aparicio, A.R., Gutiérrez-López, G.F.: Morpho-structural description of epidermal tissues related to pungency of *Capsicum* species. - J. Food Eng. **152**: 95-104, 2015.

Shand, K., Theodoropoulos, C., Stenzel, D., Dale, J.L., Harrison, M.D.: Expression of *Potato virus Y* cytoplasmic inclusion protein in tobacco results in disorganization of parenchyma cells, distortion of epidermal cells, and induces mitochondrial and chloroplast abnormalities, formation of membrane whorls and atypical lipid accumulation. - Micron **40**: 730-736, 2009.

Singh, V., Shukla, K.: Morphological and histopathological changes in papaya due to virus isolate from middle gangetic plains of India. - J. Cell Tissue Res. **12**: 3387-3393, 2012.

Teliz, D., Mora, G., Nieto, D., Gonsalves, D., García, E., Matheis, L., Avila, C.: [*Papaya ringspot virus* in Mexico] - Rev. Mex. Fitopatol. **9**: 64-68, 1991. [In Span.]

Tripathi, S., Suzuki J.Y., Ferreira, S.A., Gonsalves, D.: *Papaya ringspot virus-P*: characteristics, pathogenicity, sequence variability and control. - Mol. Plant Pathol. **9**: 269-280, 2008.

Tuo, D., Shen, W., Yang, Y., Yan, P., Li, X., Zhou, P.: Develop-ment and validation of a multiplex reverse transcription PCR assay for simultaneous detection of three papaya viruses. - Viruses **6**: 3893-3906, 2014.

Utrilla-Coello, R.G., Bello-Pérez, L.A., Vernon-Carter, E.J., Rodriguez, E., Alvarez-Ramirez, J.: Microstructure of retrograded starch: quantification from lacunarity analysis of SEM micrographs. - J. Food Eng. **116**: 775-781, 2013.

Zunjar, V., Mammen, D., Trivedi, BM., Daniel, M.: Pharmaco-gnostic, physicochemical and phytochemical studies on *Carica papaya* Linn. leaves. - Phcog. J. **3**: 5-8, 2011.